Scanning Electrochemical Microscopy. Hydrodynamics Generated by the Motion of a Scanning Tip and Its Consequences on the Tip Current

4 AUTHORS, INCLUDING:

Marc Fermigier

MINES ParisTech

71 PUBLICATIONS **1,892** CITATIONS

SEE PROFILE

Frederic Kanoufi

Paris Diderot University

119 PUBLICATIONS **1,716** CITATIONS

SEE PROFILE

Scanning Electrochemical Microscopy. Hydrodynamics Generated by the Motion of a Scanning Tip and Its Consequences on the Tip Current

Catherine Combellas,*,† Marc Fermigier,‡ Adrien Fuchs,† and Frédéric Kanoufi†

Laboratoire Environnement et Chimie Analytique, UMR 7121, ESPCI, 10 rue Vauquelin, 75231 Paris Cedex 05, France, and Physique et Mécanique des Milieux Hétérogènes, UMR 7636, ESPCI, 10 rue Vauquelin, 75231 Paris Cedex 05, France

The motion of a SECM tip above a substrate generates a flow of the surrounding fluid. Finite element calculations show that this flow is a simple linear-shear flow (Couette flow) for small tip−substrate separations and deviates from Couette's law at larger ones. The effect of fluid flow on the tip current response was determined numerically. Different mass-transfer regimes are observed depending on the insulating or conducting nature of the substrate, the tip speed (or fluid velocity), and the tip−substrate separation. Those observations are tested experimentally, and good agreement is obtained between numerical and experimental results.

For imaging purposes, the scanning electrochemical microscopy (SECM) principle consists of moving a tip at a given scan rate above a substrate and recording the variation of the electrochemical response of the sensing tip according to the geometrical or electrochemical change of the substrate. The interpretation of the experimental results is mainly based on the fact that mass transfer at an ultramicroelectrode tip is insensitive, to a certain level, to the convective fluxes generated by the tip movement. This is quite correct as long as the tip scan rate is not faster than a few micrometers per second. This condition, of course, limits the use of SECM for microlithographic purposes where rates of the order of 100 μm·s^{-1} are preferred. When SECM is used at such high scan rates, the convective field driven by the movement of the tip should not be neglected. For lithographic purposes, an immobile tip having the appropriate shape and dimensions corresponding to the desired modification would prove more convenient and as efficient; this could be performed, for example, by a band electrode.[1]

The influence of the tip movement on the tip response can be simply studied by taking into account the effect of the hydrodynamics regime generated by the movement on the electrochemical response of the tip.

As a first-order approximation, the tip displacement generates a shear flow or Couette-type flow, in which the fluid velocity varies linearly from zero at the substrate to the tip velocity at the tip surface.

Hydrodynamic electrochemistry in a Couette flow has already been analyzed from theoretical[2−11] and experimental[9−12] points of view. Systems combining electrochemistry and hydrodynamics prove interesting in different domains such as electrochemical sensors to measure wall velocities in fluid flows[13] as well as detectors in analytical systems. The latter field has considerably developed with the spread of microfluidic or channel systems combining solution flows and electrochemical detection.[14−19] However, most of these are related to 2D geometry and concern band-shaped electrodes on planar surfaces[2,8,10,11] or disk electrodes inserted in rotating cylinders.[20−25] For disk electrodes in the

(2) Newman, J. In *Electroanalytical Chemistry*; Bard, A. J., Ed.; Marcel Dekker: New York, 1973; Vol. 6, p187.

(3) Py, B.; Gosse, J *C. R. Acad. Sci. Paris A* **1969**, *269*, 401.

(4) Labbé, M.; Lebouché, M. *C. R. Acad. Sci. Paris B* **1975**, *280*, 325.

(5) Phillips, C. G. *Q. J. Mech. Appl. Math.* **1990**, *43*, 135.

(6) Zhang, W.; Stone, H. A.; Sherwood, J. D. *J. Phys. Chem.* **1996**, *100*, 9462.

(7) Stone, H. A. *Phys. Fluids A* **1989**, *1*, 1112.

(8) Geshev, P. I. *J. Electroanal. Chem.* **1996**, *410*, 1.

(9) Booth, J.; Compton, R. G.; Cooper, J. A.; Dryfe, R. A. W.; Fisher, A. C.; Davis, C. L.; Walters, M. K. *J. Phys. Chem.* **1995**, *99*, 10942.

(10) van Steenhoven, A. A.; van de Beucken, F. J. H. M. *J. Fluid Mech.* **1991**, *231*, 599.

(11) Deslouis, C.; Gil, O.; Tribollet, B. *J. Fluid Mech.* **1990**, *215*, 85.

(12) Py, B.; Duhamel, P. *C. R. Acad. Sci. Paris A* **1972**, *275*, 373.

(13) Hanratty, T. J.; Campbell, J. A. In *Fluid Mechanics Measurements*; Goldstein, R. J., Ed.; Hemisphere: Washington DC, 1983; p 559.

(14) Compton, R. G.; Coles, B. A.; Fisher, A. C. *J. Phys. Chem.* **1994**, *98*, 2441.

(15) Rossier, J. S.; Roberts, M. A.; Ferrigno, R.; Girault, H. H. *Anal. Chem.* **1999**, *71*, 4294.

(16) Rossier, J. S.; Ferrigno, R.; Girault, H. H. *J. Electroanal. Chem.* **2000**, *492*, 15.

(17) Paixão, T. R. L. C.; Camargo Matos, R.; Bertotti, M. *Electrochim. Acta* **2003**, *48*, 691.

(18) Barak-Shinar, D.; Rosenfeld, M.; Abboud, S. *J. Electrochem. Soc.* **2004**, *151*, H261.

(19) Amatore, C.; Belotti, M.; Chen, Y.; Roy, E.; Sella, C.; Thouin, L. *J. Electroanal. Chem.* **2004**, *573*, 333.

(20) Kimla, A.; Štráfelda, F. *Collect. Czech. Chem. Commun.* **1967**, *32*, 56.

(21) Gabe, D. R.; Robinson, D. J. *Electrochim. Acta* **1972**, *17*, 1121.

(22) Mohr, C. M., Jr.; Newman, J. *Electrochim. Acta* **1973**, *18*, 761.

(23) Agbangla, C.; Dumargue, P.; Humeau, P.; Morin, M. F. *Electrochim. Acta* **1981**, *26*, 1575.

(24) Legrand, J.; Dumont, E.; Commiti, J.; Fayolle, F. *Electrochim. Acta* **2000**, *45*, 1791.

(25) Mahamdia, A.; Bouabdallah, A.; Skali, S. E. *C. R. Mec.* **2003**, *331*, 245.

* To whom correspondence should be addressed. E-mail: Catherine.Combellas@espci.fr.

† Laboratoire Environnement et Chimie Analytique.

‡ Physique et Mécanique des Milieux Hétérogènes.

(1) Combellas, C.; Fuchs, A.; Kanoufi, F. *Anal. Chem.* **2004**, *76*, 3612.
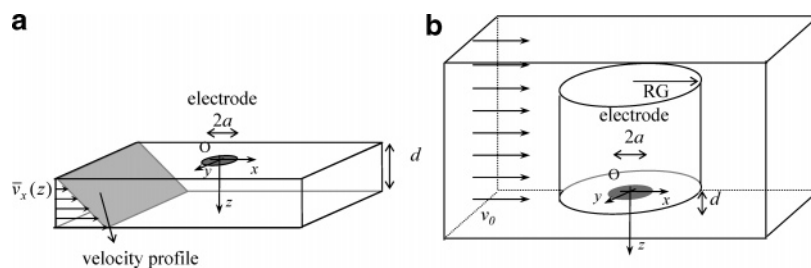
Figure 1. Schematic representation of the configuration adopted for the numerical calculation of (a) a Couette flow in a TLC configuration and (b) SECM experiments with a tip (cylinder) immobile over a substrate (bottom of the parallelepipedic cell). Cell moving at $\bar{v}_0$ in the referential of the electrode O, x, y, z.

axisymmetric geometry of the rotating cylinders or in the more demanding 3D geometry, most of the mass transfer occurs in a thin boundary layer compared to the electrode−substrate separation such that the electrode reaction is not affected by the presence of the substrate.[3,4,6,7,9]

In this work, we will investigate the hydrodynamics of a moving tip in the SECM configuration. We will show how the electrochemical tip response gives some insights on the hydrodynamic flow generated. Such electrochemical responses will be compared to numerical descriptions and flow fields obtained from the motion of tracer particles.

THEORY

First, we describe the model of the steady-state mass transport generated by a moving tip in the SECM configuration. An SECM tip is considered as a conductive disk electrode of radius a, embedded in an insulating glass sheath of radius rg, in its dimensionless form $RG = rg/a$. The tip is held at a constant distance, d, from an infinite and immobile substrate surface and moved horizontally along the x axis at a constant speed, $\bar{v}_0 = v_0\vec{\imath}$, and constant height above the fixed substrate surface. This situation is physically strictly identical to the reverse situation of an immobile tip held at a constant distance, d, from a mobile substrate moved horizontally at a constant relative speed, $\vec{\bar{v}}_0 = -\bar{v}_0 = -v_0\vec{\imath}$. For both situations, to obtain a steady-state solution of the mass-transfer processes toward the electrode, the calculation has to be done in the electrode reference frame.[22] In the rest of this work, outlined velocities, such as $\bar{v}$, will refer to velocities in the electrode reference frame (O, x, y, z, where O is the center of the electrode, see Figure 1). They are simply obtained from the velocity in the reference frame of the cell, denoted v, by

$$\bar{v} = v_0 - v \tag{1}$$

The relative movement of the substrate surface provides a flow of the electrolytic solution with it and the velocity of the fluid at each point of the solution $M(x,y,z)$ is given by $\bar{v}(\bar{v}_x, \bar{v}_y, \bar{v}_z)$. In the diffusion region located between the tip and the substrate we show, as discussed later, by numerical estimation of the velocity field, that the velocity is directed only along the x axis and that the velocity along the x direction is dependent on the height z, $\vec{\bar{v}} = \bar{v}_x(z)\vec{\imath}$.

In the special case of large values of RG ($RG \gg L$, with $L = d/a$), the so-called thin-layer cell (TLC) setup, the movement of

the electrode surface leads to the development of a simple Couette flow between the substrate and the tip, and at each point

$$\bar{v}_x(z) = v_0 z/d \tag{2}$$

where v_0/d represents the fluid shear rate. In the case of the SECM, the linear variation (2) between $\bar{v}_x$ and z might not be observed mainly since the electrode surface is not infinite; this is especially the case on the edge of the tip but also in the center of the tip for the highest values of L/RG ($L = d/a$.).

One aim of this work is to determine numerically the velocity profile of the fluid under SECM experiments. The flow field, $\vec{\bar{v}}$, is calculated by solving the steady-state laminar Navier−Stokes equations for an incompressible, isothermal, and Newtonian fluid. The mass conservation equation is

$$\vec{\nabla}\cdot\vec{\bar{v}} = 0 \tag{3}$$

where $\vec{\nabla}$ is the three-dimensional operator of coordinates ($\partial/\partial x$, $\partial/\partial y$, $\partial/\partial z$). Then the momentum conservation equation writes

$$\rho(\bar{v}\cdot\vec{\nabla})\vec{\bar{v}} = \eta\nabla^2\vec{\bar{v}} - \nabla\vec{P} \tag{4}$$

where ρ and η are respectively the density and the dynamic viscosity of the fluid and P is the static pressure of the fluid. From the resolution of (3) and (4) in 3D, one might obtain the flow field generated by the tip displacement in the fluid. This velocity field is then used for the evaluation of the concentration distribution in the SECM cell.

The fluid consists of an electrolytic solution containing an electroactive species A at concentration C and an electrolyte in sufficient concentration so that migration effects can be neglected. The electrode is held at a potential such that the electrode reaction involves an exchange of n electrons per A:

$$A \pm ne^- \rightarrow B$$
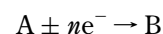
The electron exchange is controlled by mass transfer, the concentration of A being null at the electrode surface while C tends toward C_0, the bulk concentration, far away from the electrode.

In the electrode reference frame, the steady equation of transport is

$$D\frac{\partial^2 C}{\partial x^2} + D\frac{\partial^2 C}{\partial y^2} + D\frac{\partial^2 C}{\partial z^2} - (\vec{v}\cdot\vec{\nabla})C = 0 \qquad (5)$$

where D is the diffusion coefficient of A. The steady tip current, i_T, is given by grad C at the electrode surface.

Most of the numerical and analytical solution of (5) concerns the special case of 2D geometry where the electrode is a strip (no variation along the y axis). And the only works[4–7,9] involving resolution of the (heat or species) diffusion equation in 3D geometry cannot be applied to the SECM conditions as the main boundary condition is that most of the mass transfer occurs within a thin layer as compared to the electrode−substrate separation, d. However, this asymptotic situation might be observed within the SECM or TLC setup under appropriate conditions. They depend on two dimensionless parameters: the Péclet number, $Pe = v_0 d/D$, that characterizes the ratio of convective transport to diffusive transport and the normalized tip−substrate distance $L = d/a$.

In the present case, it is more convenient to define a shear Péclet number, $P_s = Pe/L^2$ that characterizes the ratio of convective to diffusive transport in a thin mass transport layer, such that the dimensionless form of eq 5 is

$$\frac{\partial^2 c}{\partial X^2} + \frac{\partial^2 c}{\partial Y^2} + \frac{\partial^2 c}{\partial Z^2} = P_s\left(\frac{\bar{v}_x}{v_0}\frac{\partial c}{\partial X} + \frac{\bar{v}_y}{v_0}\frac{\partial c}{\partial Y} + \frac{\bar{v}_z}{v_0}\frac{\partial c}{\partial Z}\right) \qquad (6)$$

where $c = C/C_0$, $X = x/a$, $Y = y/a$, and $Z = z/a$ are respectively the corresponding dimensionless variables.

The experimentally measurable quantity in this problem is the tip current, i_T. It is convenient to use its dimensionless form, I_T. SECM literature[26] generally normalizes the tip current by the steady-state current in the bulk solution (infinite distance from the substrate), $i_{T,\infty} = 4nFC_0Da$, where F is the Faraday constant. The dimensionless current is[27]

$$I_T = i_T/i_{T,\infty} \qquad (7)$$

THEORETICAL RESULTS

As discussed above, the momentum and mass transfer are solved, under steady-state conditions, in the electrode reference frame. Figure 1 represents respectively the thin-layer cell, TLC (a) and SECM (b) configurations. For an easier comparison with experimental results, we have presented all the simulation curves related to the velocity field in the cell reference frame.

Flow Generated by a Moving Tip. In the SECM configuration, deviations from the Couette approximation are expected because of the finite dimension of the electrode glass sheath. The numerical resolution of Navier−Stokes' eqs 3 and 4 gives an estimate of these deviations and their influence on the tip current.

Cell Configuration and Boundaries. We have used a finite elements method to perform the numerical simulations (software package FEMLAB version 3.0, Comsol France, Grenoble, France). The computation volume is a parallelepipedic cell of square base

(26) Mirkin, M. V. In *Scanning Electrochemical Microscopy*; Bard, A. J., Mirkin, M. V., Eds.; Marcel Dekker: New York, 2001; Chapter 5, p 145.
(27) In the mass- (and heat)-transfer literature, the dimensionless Nusselt (or Sherwood) number, Nu, is preferred: $Nu = i_T/nFC_0Da = 4\,I_T$.

1×1 mm^2, height 1.5 mm. The electrode is a cylinder with variable diameter and height (see Figure 1b for a schematic representation of the cell + electrode). The distance between the bottom of the cell and the electrode is still d. Four values of d have been chosen to compare simulations and experiments: $d = $ 17, 68, 125, and 260 μm. The active part of the electrode is a 50-μm-diameter disk, which, in the simulation framework, will be treated as the intersection of the electrode itself (metallic disk + insulating sheath) and a 50-μm-diameter cylinder located exactly below the metallic wire. Different cylinders, located around and under the electrode, were used to force a finer meshing in the area congruent to the electrode and especially in the interspace between the electrode and the bottom of the cell. The meshing of the volume for hydrodynamic studies generated a minimum of 9×10^3 cells.

For the simulation of the Navier−Stokes' equations, we have taken for the density and the dynamic viscosity of the solvent, respectively, $\rho = 10^3$ kg m^{-3} and $\eta = 10^{-3}$ kg m^{-1} s^{-1} (water). The following values were imposed: for the whole electrode $\vec{v}(x,y,z) = 0$ (no slip); for the cell walls, $\vec{v} = v_0$, except for the wall opposite the movement, which is set as an outflow with a condition on the pressure ($p = 0$) so that there is no viscous stress on the fluid at this outlet. The calculations were performed for small values of the Reynolds number, $Re = \rho v_0 d/\eta$, as its maximum value is obtained for the largest value of $d = 260$ μm when $v_0 < 200$ μm s^{-1}, which leads to $Re \leq 1.56 \times 10^{-1} \ll 1$.
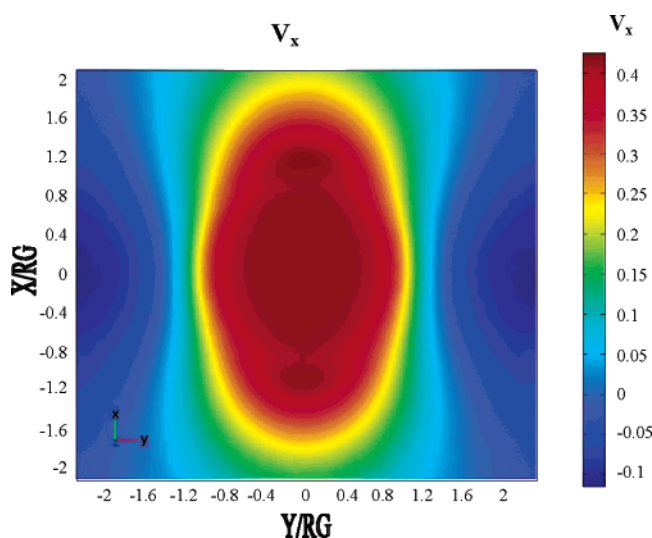
Validity of the Model. For a given electrode−substrate distance, d, the velocity field, $\vec{v}$, inside the cell may depend on the cell size and the electrode height. However, we are interested in the effect of the velocity field on the tip current, which itself should only depend on the velocity field beneath the electrode. We have assumed that the cell size and electrode height had little influence on the velocity field under the electrode. We have tested this assumption for extreme values of these parameters. For the smallest cells (or the highest electrodes), the velocity field around and above the electrode is higher due to mass conservation. Nevertheless, this results in a negligible effect on the velocity field and the tip current under the electrode. We have checked that the velocity field, $\vec{v}$, obtained by simulation for a given d is independent of the value of the velocity v_0. Indeed, the dimensionless velocity fields obtained for two values of v_0 differ from less than 0.01%. This is a consequence of the low Reynolds number. For $Re \ll 1$, the streamlines are unchanged when changing the velocity modulus, whatever the system geometry.

Velocity Field in an SECM Experiment. The numerical resolution of Navier Stokes' equation gives $\vec{v}$ at any point of the cell. We have shown that in the domain of importance (region between the electrode and the substrate) the main contribution to the velocity field is $\bar{v}_x$. For an easier and clearer comparison with experimental data, we have presented the profile of v_x, the velocity of the fluid, in the referential of the cell. Figure 2 shows the dimensionless velocity, $V_x = (v_0 - \bar{v}_x)/v_0 = 1 - \bar{V}_x$ along the vertical of the electrode center as a function of the dimensionless distance, $z/d = Z/L$, for $d = 17$, 68, 125, and 260 μm ($L/RG = 0.068$, 0.272, 0.5, and 1.04, respectively). The straight line corresponds to the Couette flow. When d increases, the profile, which is quasi-linear for $d = 17$ μm, deviates progressively from linearity.
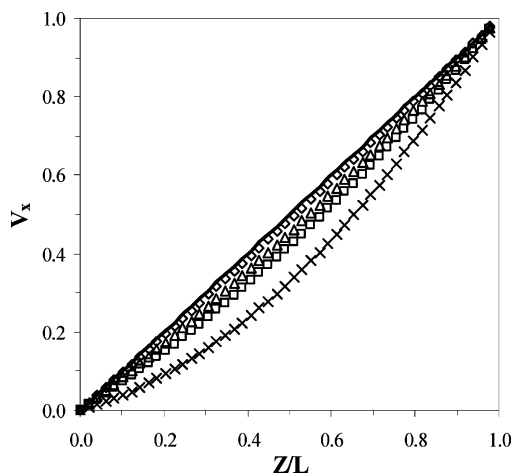
Figure 2. Simulation of the velocity profiles along the z axis. $v_0 = 500\ \mu m\ s^{-1}$. $d = 17$ ($\diamond$), 68 ($\triangle$), 125 ($\square$), and 260 μm ($\times$) ($L/RG = 0.068$, 0.272, 0.5, and 1.04, respectively). Straight line, Couette flow.

Figure 3. Simulation of the velocity profiles in the x,y plane of equation $Z = 0.5$ for $d = 100\ \mu m$.

Similar trends are observed in the whole region under the electrode, and the deviation from linearity is more important near the edge of the electrode. In the case of the short distance $d = 17\ \mu m$, the profile is no longer linear at the edge of the electrode.

The variation of the velocity in the X,Y plane of altitude $Z = 0.5$ is represented for $d = 100\ \mu m$ in Figure 3. In both directions, when leaving the region under the electrode, the only constraints on the solvent are those from the cell walls and the top of the liquid. Along both directions, the velocity profile develops outside the electrode area. Indeed, in any horizontal plane sectioning the electrode, the fluid movement develops far from the electrode over a boundary layer of the order of $(\eta r g/\rho v_0)^{1/2} \sim 0.3\ (a/v_0)^{1/2}$ (in cm).[28] Even for v_0 (in $\mu m\ s^{-1}$) $> 100\ a$ (in μm), the boundary layer in which the flow develops outside the electrode is $\sim 300\ \mu m$. Therefore, the fluid moves in a region much larger than the electrode−substrate separation, as observed in Figure 3. Moreover, the fluid movement develops in a much wider area along the axis for the flow (x axis) than along the y axis as the fluid is

(28) *Boundary-layer Theory*, 7th ed.; Schlichting, H. Ed.; McGraw-Hill: New York, 1979.

almost immobile at $Y = 1.4RG$. The velocity is approximately constant for $|Y/RG| < 0.8$ and then decreases and reaches 0 at $|Y/RG| = 1.4$. For higher $|Y/RG|$ values, the negative velocity results from the small size of the cell used for the calculation and then from the closeness of the walls of the cell. Along the x axis, which is the axis for the flow, the velocity is much less dampened, and near the edge of the glass sheath ($|X/RG| \sim 1$), an inflection point is observed that corresponds to a pressure extremum.

Electrochemistry at a Disk Microelectrode in a TLC with a Couette Flow. Cell Configuration and Boundaries. The FEMLAB software also proved efficient to solve SECM problems.[29,30] We used a parallelepipedic cell, schematically depicted in Figure 1a, of square base $1 \times 1\ mm^2$ and various electrode−substrate separations, d. The electrode is a disk of radius $a = 25\ \mu m$ centered on the square surface. We have checked that similar results were obtained after homothetic resizing of the cell dimensions. For higher refinement of the three-dimensional mesh, we used a geometrical expansion along the z axis. The meshing of the cell generated a minimum of 10^5 cells.

As mentioned earlier, the flow was considered as a Couette's one and the velocity is given by (2). The steady-state diffusion equation resulting from (2) and (6) ensues:

$$\frac{\partial^2 c}{\partial X^2} + \frac{\partial^2 c}{\partial Y^2} + \frac{\partial^2 c}{\partial Z^2} = P_S Z \frac{\partial c}{\partial X} \tag{8}$$

It was solved according to the following boundary conditions. $c = 1$ on each vertical wall of the cell. Plane $Z = 0$: $c = 0$ on the electrode disk and $\partial c/\partial Z = 0$ outside the disk. Plane $Z = L$: $c = 1$ for a conducting substrate and $\partial c/\partial Z = 0$ for an insulating substrate.

The tip current is obtained in its dimensionless form from the concentration distribution as

$$I_T = \int_{X^2+Y^2\leq 1}\int \frac{\partial c}{\partial Z}\Big|_{Z=0}\ dX\ dY \tag{9}$$

RESULTS AND DISCUSSION

Figure 4 represents the numerical results obtained for different values of the velocity, $10^{-5} < v_0$ (cm s^{-1}) < 2, different tip−substrate separations, $0.28 < L < 14$, different electrode radii (12.5 and 25 μm), and an insulating or a conductive substrate. They are presented as the logarithmic variations of the dimensionless electrode current, I_T, as a function of the Péclet number, P_s. We have observed that I_T depended only on the normalized tip−substrate distance, L, the nature of the substrate, and the Peclet number, P_s but was independent of the tip radius, a.

This bundle of curves shows trends similar to those obtained for the transient establishment of the steady tip current in SECM.[31−33] The curves exhibit different kinetic regimes depending
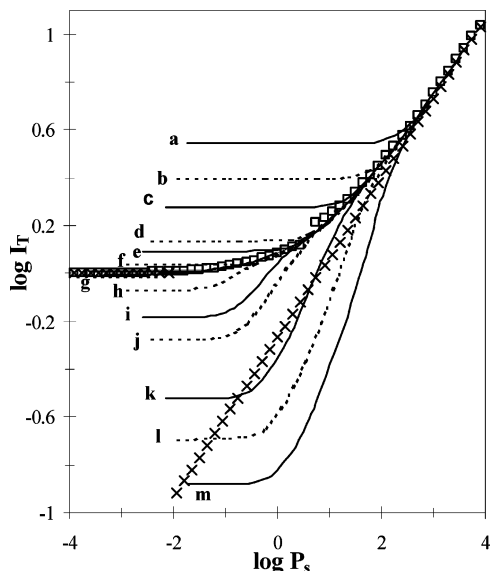
(29) Xiong, H.; Guo, J.; Kurihara, K.; Amemiya, S. *Electrochem. Commun.* **2004**, *6*, 615.

(30) Dobson, P. S.; Weaver, J. M. R.; Holder, M. N.; Unwin, P. R.; Macpherson, J. V. *Anal. Chem.* **2005**, *77*, 424.

(31) Bard, A. J.; Denuault, G.; Friesner, R. A.; Dornblaser, B. C.; Tuckerman, L. S. *Anal. Chem.* **1991**, *63*, 1282.

(32) Unwin, P. R.; Bard, A. J. *J. Phys. Chem.* **1991**, *95*, 7814.

(33) Bard, A. J.; Mirkin, M. V.; Unwin, P. R.; Wipf, D. O. *J. Phys. Chem.* **1992**, *96*, 1861.

Figure 4. Simulation curves in the configuration of a thin-layer cell (Couette's configuration). Conductive substrate: $d/a = 0.28$ (a), 0.44 (b), 0.68 (c), 1.4 (d), 2.0 (e), 5.0 (f), and 20 (g). Insulating substrate: $d/a = 20$ (g), 5.0 (h), 2.0 (i), 1.4 (j), 0.68 (k), 0.44 (l), and 0.28 μm (m). $a = 12.5$ and 25 μm. Analytical expressions: from Stone and Phillips ($\square$); from Lévêque ($\times$).

on the values of P_s and L and collapse on a single curve (g) at large values of P_s. At hand, distinction between the different mass-transfer regimes might be obtained from comparison of the different characteristic dimensionless lengths of the problem, which are similar to the characteristic dimensionless times, T_c, reported in previous analyses of the transient SECM responses.[31,32]

Effect of Shear Flows on an Isolated Disk Microelectrode. The master curve (g) corresponds to the case of an electrode held at a very large distance from the substrate ($L = d/a \gg 1$, here $L \sim 14$) and submitted to a shear flow.

This curve presents different mass-transfer regimes according to the values of P_s. Two asymptotic behaviors are observed. At low values of the Péclet number P_s, the convective field generated by the flow is not important enough to perturb the diffusive mass transfer toward the microelectrode. The right-hand side of the transport equation (8) can be neglected, and we observe the current of a microelectrode in static solution. The current is constant and $I_T = 1$ at low P_s. Increasing the velocity increases the convective mass transport; consequently, the microelectrode current is affected and it increases for increasing scan rates (intermediate regime).

In the other limiting case of fast velocities, the convection characteristic length is much thinner than the electrode dimension, a, the diffusion process is quasi-linear over the z axis, and derivatives over X and Y (left-hand side of eq 8) can be neglected. This asymptotic situation has been solved analytically by Lévêque (Figure 4, x),[34] and I_T is expected to increase as the one-third root of the velocity:

$$I_T = \frac{3(6)^{1/3}\Gamma(1/3)}{20\Gamma(2/3)}P_s^{1/3} \approx 0.53_9 P_s^{1/3} \qquad (10)$$

where Γ is the gamma function.

Equation 10 shows that the diffusion layer thickness that characterizes the mass transport along the z axis is related to the Péclet shear number,[2] P_s, and in its dimensionless form

$$\lambda_z = l_z/a \sim P_s^{-1/3}$$

Therefore, the asymptotic Lévêque's behavior is expected when this length is small compared to the electrode size: $P_s^{-1/3} \ll 1$. This is observed for values of $P_s > 1000$ (asymptotic curve from Lévêque represented as the dotted line, $+$, in Figure 4). Similarly, the convective mass transport is negligible when its characteristic length is of the order of the electrode dimension: $\lambda_z > 1$ and then $P_s < 1$.

For intermediate velocities and P_s numbers, radial diffusion along the edges of the electrode interferes and eq 8 becomes three-dimensional. The similarity of (8) to transient diffusion equations allows us to define the characteristic length of radial diffusion along the edges of the electrode as $\lambda_{xy} \sim P_s^{-1/2}$. Deviations from Lévêque's law should be observed when axial and radial diffusion lengths are comparable, as observed in Figure 4 for $10^{-2} < P_s < 10^3$.

Two asymptotic analytical solutions ($\square$ in Figure 4) have been developed by Phillips[4,35] for low P_s numbers ($P_s < 1$) and by Stone[7,35] for higher values in the special case of noninteracting substrates ($P_s^{-1/2}$ or $P_s^{-1/3} \ll L$). The agreement with these expressions is good for values of $P_s < 1$ or $P_s > 40$. However, the analytical expressions that best fit our numerical results within less than 0.1% for all P_s values fulfill the set of equations reported in ref 35.

Influence of the Substrate. When a substrate is introduced in the vicinity of the microelectrode, the microelectrode might sense its presence accordingly owing to its nature (conductive or insulating).

However, limiting cases might be observed too. When the axial and radial mass-transfer lengths are much thinner than d, the tip, again, does not sense the substrate and the tip current is governed by equations in ref 35. Conversely, as soon as λ_{xy} or λ_z is of the order of L, the electrode senses the presence of the substrate and the tip current deviates from these equations. We have found that the tip does not sense the substrate, for the whole set of tip–substrate separations investigated, when empirically $\lambda_{conv} \sim P_s^{-1/2} + P_s^{-1/3} \leq 0.61_6 L$. For lower velocities, at a given L, and then lower values of P_s, the mass transport to the electrode is perturbed by the presence of the substrate and the substrate is, to some extent, sensed by the tip.

For a conductive substrate held at a given distance L from the tip, when decreasing the velocity, the tip current tends toward a limiting case where it is controlled by the feedback reaction. The current value, $I_{T,c}$, observed in the absence of convection is then given by the expression[26]

(34) Lévêque, M. A. *Ann. Mines* **1928**, *13*, 201.
(35) Phillips' expression[5] at low P_s ($P_s < 1$) is $I_T = (1 - 0.02817P_s^{3/2})/(1 - 0.20281P_s^{1/2})$ since Stone's expression[7] gives for $P_s > 100$: $I_T = 0.5393P_s^{1/3} + 0.8875P_s^{-1/6}$. In our case, the analytical expressions that fit the best our numerical results are the following: for $P_s < 1$, $I_T = (1 - 0.539P_s^{3/2})/(1 - 0.199P_s^{1/2})$; for $1 < P_s < 40$, $I_T = 0.337P_s^{0.40} + 0.774P_s^{-0.028} + 0.099$; for $P_s > 40$, $I_T = 0.539P_s^{1/3} + 0.888P_s^{-1/6}$.

$$I_{T,c} = 0.745 + 0.758/L + 0.235 \exp(-1.683/L) \quad (11)$$

This situation is reached when the convective length, λ_{conv}, is larger than the size of the tip−substrate gap, L. We have found empirically that the substrate feedback could be considered as unperturbed by the tip movement as long as $\lambda_{conv} \sim P_s^{-1/2} + P_s^{-1/3} \geq 1.59L$.

Similarly, for an insulating substrate, when decreasing the velocity, the tip current decreases toward its value in the absence of flow. The current is then controlled by the blocking of axial diffusion by the substrate; it depends strongly on RG and L.[26] Therefore, the domain of P_s values for which the electrode is only controlled by the hindering substrate should be strongly dependent on L and RG. We have shown empirically that for $0.2 < L < 2.7$ the velocity had no effect on the current of a microelectrode held in the vicinity of an insulating substrate if $P_s^{-1} \geq 14.4L$. This expression corresponds, in terms of electrode velocity, to $v_0 a/D \leq 0.06$, and occurs for low P_s values as the diffuse layer spreads in a wider domain than in the case of a conductive substrate. Larger values of P_s correspond to an increase of the current as the process is controlled by mixed diffusion/convection.

SECM. Effect of the Tip Motion on the Tip Response. *Cell Configuration and Boundaries.* The same boundary conditions as that for the case of the TLC have been used. The whole cell is meshed more finely, especially in the vicinity of the disk electrode, than for the calculation of the velocity field as a higher precision is required for the calculation of the tip current. A minimum of 3 × 10^4 mesh points is used. The velocity on the points of this new mesh was estimated by extrapolation from the values in the previous mesh.

Influence of the Tip−Substrate Distance and the Electrode Glass Sheath Radius on the Tip Current. Figure 5 presents the logarithmic variations of I_T, as a function of the apparent Peclet number, $P_s = v_0 a^2/dD$, obtained by numerical simulation for different values of v_0 (10^{-3} μm s^{-1} < v_0 < 500 μm s^{-1}), d (17, 68, 125, and 260 μm), and $a = 25$ μm and for insulating and conductive substrates. In the insulating case where $d = 17$ and 260 μm, we have also studied the influence of RG (5, 10, 15).

In all cases, the variations of the current are similar to those observed with a thin layer cell under a Couette flow.

For insulating substrates, the three TLC characteristic regimes are followed.

In the case of a short electrode-substrate distance, such as $d = 17$ μm ($d/a = 0.7$) and $P_s < 0.3$, we observe that the current is higher in the SECM configuration (Figure 5, small, medium, and large squares) than for a thin-layer cell (Figure 5, curve j). This can be explained by the occurrence of diffusion at the edges of the electrode, which results in a smaller hindrance to diffusion due to the glass sheath than in the case where the electrode plane is infinite (actually $RG = 14$). At such short distance, when RG increases, diffusion becomes more hindered and the situation tends toward that of TLC, this occurs for smaller P_s when RG is higher (Figure 5, small, medium, and large squares). For $P_s > 40$ when convection becomes predominant, the SECM profile is the same as that of Couette in TLC since at such distances, velocity profiles are linear (Figure 2, $\diamond$). For intermediate P_s ($1 < P_s < 40$), the ratio d/rg is too high for convection/diffusion from the edge of the electrode to affect significantly the current.
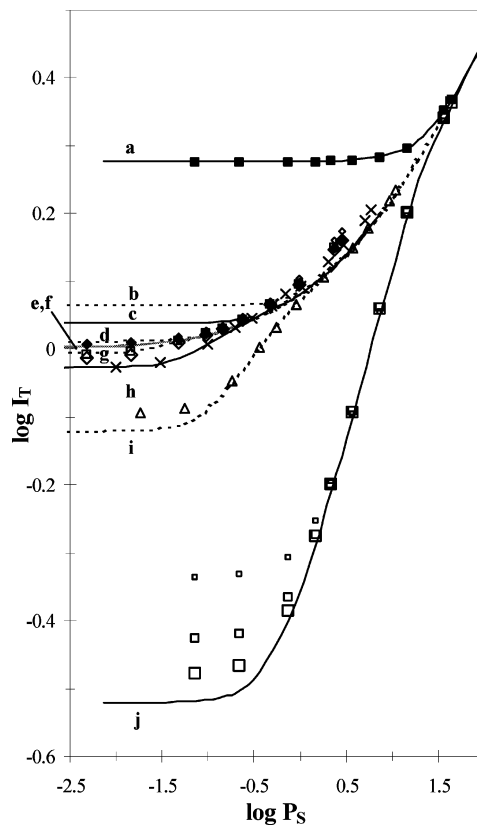
Figure 5. Simulation curves in the configuration of a thin-layer cell (Couette's configuration). Conductive substrate: $d = 17$ (a), 68 (b), 125 (c), 260 (d), and 500 μm (e). Insulating substrate: $d = 500$ (f), 260 (g), 125 (h), 68 (i), and 17 μm (j). Simulations in the SECM configuration. Conductive substrate: $d = 17$ μm, $RG = 10$ (■); $d = 260$ μm, $RG = 10$ (◆). Insulating substrate: $d = 260$ μm, $RG = 5$ (small tilted square), 10 (medium tilted square), and 15 (large tilted square); $d = 125$ μm, $RG = 10$ (×); $d = 68$ μm, $RG = 10$ (△); $d = 17$ μm, $RG = 5$ (small square), 10 (medium square), and 15 (large square).

When the electrode−substrate distance increases, diffusion becomes less hindered and at 260 μm, there is nearly no hindrance at all. For small P_s, there is no significant difference between the TLC configuration (Figure 5, curve g) and that of the SECM whatever RG (small and medium tilted squares). Conversely, for higher P_s, because of the nonlinearity of the velocity profiles at such distance (Figure 2, □), differences between the two configurations are observed. The current deviation from the generic Couette curves reflects that the value of the velocity gradient, the shear rate $dv_x/dz|_{z=0}$, at the electrode surface, is higher than the Couette's one (v_0/d). Taking into account the nonlinearity of the velocity profile in the calculation of P_s, $P_s = dv_x/dz|_{z=0}a^2/D$, fits the generic Couette curves.

For conducting substrates, the two TLC characteristic regimes are also followed. For $d = 17$ μm, no difference between the two regimes is observed. Conversely, for higher d, deviations from linearity are observed. In a way similar to that reported for the insulating substrate, for a given P_s, they result from the highest velocity gradient, which implies higher currents.

Practical Consequences. From a practical point of view, SECM is often used as an imaging[36] or a constructing tool[37,38] for L values of the order of 0.3−0.7. The maximum tip velocity that can be considered as having a negligible effect on the fluid displacement

and hence on the mass transport toward the electrode above an insulating substrate is dependent on the species diffusion coefficient, D, and the tip radius, a, and is $\sim$0.06 D/a, that is $\sim$3 μm s^{-1} for $D = 5 \times 10^{-6}$ cm^2 s^{-1} and $a = 10$ μm. Above a conductive substrate, the maximum speed depends also on d, the value of the tip–substrate separation, and is between 140 and 500 μm/s (for, respectively, $L = 0.7$ and 0.3) for $D = 5$ 10^{-6} cm^2 s^{-1} and $a = 10$ μm.

For higher speeds, the tip current contains a part of convective mass transfer, and the apparent reactivity of the substrate surface, when such effects are not taken into account, is certainly overestimated in imaging applications. For speeds higher than 1.3 and 6.3 mm s^{-1} (for, respectively, L = 0.7 and 0.3), no difference in the tip current is observed between conductive and insulating substrates, and the tip current loses its ability to discriminate between differences in substrate reactivity (insulating versus conducting).

For electrochemical etching of surfaces in the feedback mode, the same conclusions might be drawn. The etching of poorly reactive surfaces (near insulating behavior) requires low tip rates ($v_0 < 10$ μm s^{-1}) to maximize the concentration of the electrogenerated etchant at the substrate surface.

Finally, the lateral motion of the SECM tip induces a local pressure difference on the substrate. At hand, the pressure difference between the front and the end part of the electrode is

$$\Delta P = \eta \frac{2RG}{L^2} \frac{v_0}{a} \qquad (12)$$

It corresponds typically to small pressure fractions of Pa. Moreover, this might be of importance for the investigation of deformable interfaces such as liquid–liquid, liquid–air interfaces and lipidic bilayer membranes. Indeed, the pressure difference caused by the electrode displacement might deform such a soft interface. The deformation of a soft interface is compensated by the capillary pressure, P_c, of the interface which is

$$P_c = \gamma/R \qquad (13)$$

where γ is the interfacial tension and R the radius of curvature of the deformed interface. The resulting spherical deformation has the dimension of the electrode assembly of radius RG and height h; then, one could approximately consider that $R \sim 4$ RG^2/h. It then ensues from combination of (12) and (13) that the deformation height is

$$h \sim \frac{\eta v_0}{\gamma} d\left(\frac{2RG}{L}\right)^3 \qquad (14)$$

Soft interfaces such as water–oil interfaces exhibit interfacial tensions, γ_0, of the order of 10–30 mN cm^{-2} and the deformation of the interface induced by the movement at $v_0 = 10$ μm s^{-1} of a

(36) *Scanning Electrochemical Microscopy*; Bard, A. J., Mirkin, M. V., Eds.; Marcel Dekker: New York, 2001.
(37) Mandler, D. In *Scanning Electrochemical Microscopy*, Bard, A. J., Mirkin, M. V., Eds.; Marcel Dekker: New York, 2001; Chapter 13, pp 603–627.
(38) Kanoufi, F.; Combellas, C.; Shanahan, M. E. R. *Langmuir* 2003, *19*, 6711–6716.

25-μm-diameter electrode, held at $L = 0.5$, corresponds to a dip 0.1–0.03 μm high. However, the use of a tensioactive electrolyte that lowers the interfacial tension, in liquid–liquid interface studies, or imaging interfaces at lower L separation might cause more severe modifications of the investigated interface and would result in incorrect data interpretations.

EXPERIMENTAL SECTION

All chemical reagents were purchased from Aldrich (Saint-Quentin Fallavier, France) and used as received. The solvent was ultrapure water that was obtained in the laboratory (Milli-Q grade) or DMF (puriss, Aldrich). Platinum wires, used in the ultramicroelectrodes, were of 99.9% purity (Goodfellow). Ultramicroelectrode (metallic radius, $a = 25$ μm, ratio of glass-to-metallic radii, RG (5 < RG < 10) tips were obtained according to the literature.[39] Due to successive polishings of the electrode, the value of RG may vary in a series of experiments with the same electrode.

Motion of Fluorescent Particles. To determine the velocity field of a solvent (water) beneath the electrode when the latter is moved parallel to a substrate surface, we have added tracer particles to the solvent and observed them through an inverted microscope. The suspension of the particles (fluorescent polystyrene particles: density 1.05, diameter 1 μm) in water was put into a quartz parallelepipedic cell of rectangular base 30 × 35 mm^2 centered above the microscope objective. The electrode, immersed into the solution, was moved vertically and horizontally with two motorized translation stages (CMA step motors driven by a computer-controlled ESP300, Newport). The parallelism of the electrode trajectory and the bottom of the cell (substrate) were adjusted with a motorized goniometer (Newport) and checked by optical measurement of the electrode–substrate distance at two points distant of 1 mm or electrochemical measurements (see next section).

The microscope operates with a UV lamp equipped with a filter (GFP filter) in order to specifically excite the particles at their emission wavelength. It is connected to a CCD camera (Cohu 1100 series) controlled by a PC (piloted by the Scion freeware). The focal plane is adjusted by changing the distance between the objective and the electrode, allowing the visualization of the particles within the depth of field. The velocity is obtained as the particle mean displacement on successive frames. The frequency of the image acquisition is set such that the time of flight of the whole electrode ($\sim$400 μm) is represented by 100–160 images.

Such a setup is commonly used in fluidics for larger cells and translation speeds. In our case, its limitations are mainly due to the dimensions of the experiment and result in a decrease of the contrast. First, the particles size is not negligible compared to the shortest electrode–substrate distances used. Second, the particles sediment slowly to the cell bottom. Some consequences ensue: (i) if too many particles sediment, there may be not enough particles to visualize in a given focal plane; (ii) the accumulation of particles in the cell bottom increases dramatically the light noise, which interferes with images near the substrate surface; (iii) same as (ii) for the electrode surface, which may retain particles at the beginning of the experiment when the electrode is in contact with the substrate; and (iv) because of gravity, the vertical position of a particle may change as time goes on. Third, natural convection due to interfering vibrations might take place since the setup is not isolated from the outside by an

antivibration table. For all these reasons, it is difficult to discriminate objective translations smaller than 10 μm. Confocal microscopy might help resolve smaller increments.

Electrochemistry at a Moving Tip. The experimental setup was the same as in the latter part except that the fluorescent particles were replaced by an electroactive species (Fe(CN)$_6^{4-}$ or phthalonitrile) in an electrolytic solution (aqueous 0.1 M KCl or DMF + 0.1 M NBu$_4$BF$_4$). Electrochemical measurements were performed in 10−25 mL of solution with a classical three-electrode setup composed of a platinum microelectrode tip (metallic radius, $a = 25$ μm, ratio of glass-to-metallic radii, RG = from 8.9 to 7.6, a platinum counter electrode (radius 0.5 mm) and an anodized Ag/AgCl reference wire (radius 0.5 mm) without any reference compartment. Potentials were imposed and currents measured by a potentiostat/galvanostat (CH660A, CH Instruments). The mass-transfer controlled current for either Fe(CN)$_6^{4-}$ oxidation or phthalonitrile reduction at the potential of, respectively, 0.4 or −1.8 V versus Ag/AgCl was analyzed.

Three electrochemical cells were tested, the bottom of the cell acting as the substrate: a cylindrical cell with a convex bottom, a quartz cubic cell with a flat bottom, and a plastic Petri box. With the latter cell, only measurements at $d = 260$ μm were performed since its bottom surface was too rough to be used for measurements with smaller d. The quartz cell exhibited the best surface state.

First, the parallelism between the electrode and the substrate (cell bottom) was adjusted with a motorized goniometer by checking that the current was constant during a translation displacement of the electrode above the substrate at a constant height ($v_0 = 100$ μm s^{-1}, $t = 50$ s, displacement distance 5 mm). The translation speed is higher than the 10 μm s^{-1} required for a purely diffusive regime, but the tip−substrate separation is small enough ($L < 0.4$) to ensure that the tip current is sensitive to the presence of the substrate and in the mixed control regime.

The initial vertical positioning of the electrode was obtained by adjusting the ratio of the current to its value at infinite distance from the substrate to its analytical expression for $RG = 10$.[26] For $d = 125$ and 260 μm, we first positioned by the electrochemical method the electrode at $d = 17$ μm and then moved it upward to the desired position.

For the measurements in diffusion/convection experiments, first, the potential was applied to the steady electrode until a steady current was observed for ∼100 s and then the electrode was moved parallel to the substrate surface at a constant speed, v_0.

In such experiments, some error sources are worth mentioning: the substrate surface state, the insufficient electrode planarity, the current drift due to the slow passivation of the electrode, the inaccuracy in RG value, and the approximate parallelism between the electrode and the substrate. Such defects result in errors generally lower than 2−4%. The two latter effects result in an inaccurate determination of d, which is critical mainly for small d.

RESULTS AND DISCUSSION

Most of the experiments were performed by moving the electrode, the substrate remaining still. One experiment was performed in the reverse situation to confirm that it gave similar results.
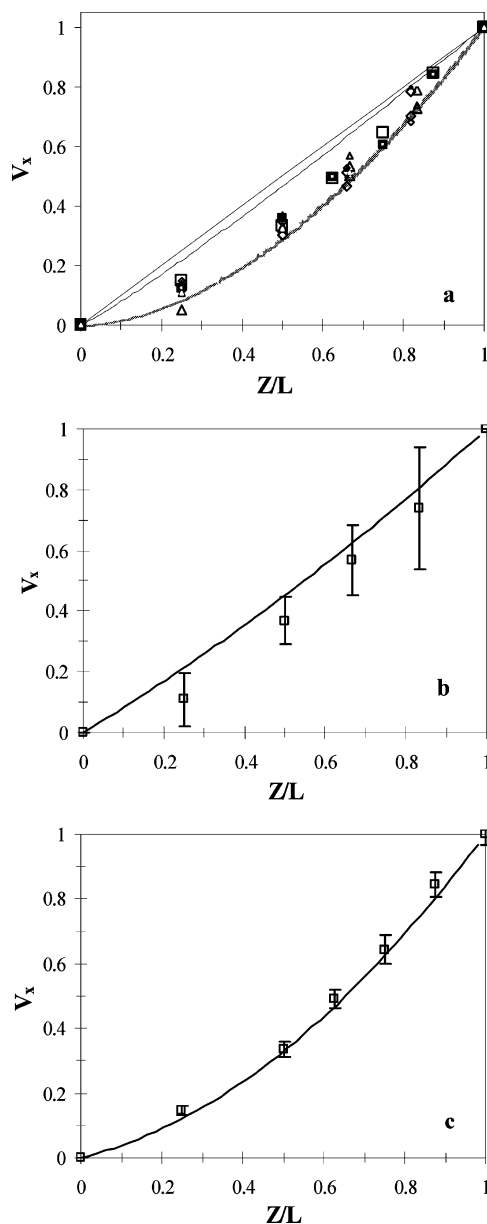
Figure 6. Experimental velocity profiles (a) $d = 68$ μm, $v_0 = 30$ (small triangle), 50 (medium triangle), and 100 μm s^{-1} (large triangle). $d = 125$ μm, $v_0 = 30$ (small tilted square), 50 (medium tilted square), and 100 μm s^{-1} (large tilted square). $d = 260$ μm, $v_0 = 30$ (small square), 50 (medium square) and 100 μm s^{-1} (large square). Power laws, $v/v_0 = (z/d)^B$: - - - ($B = 1.1$); — ($B = 1.8$). Comparison of experimental and simulated profiles (b, c) —, simulated profile; □, experimental points. $d = 68$ (b) and 260 μm (c).

Motion of Fluorescent Particles. Velocity Field. The normalized velocity, v/v_0, is represented in Figure 6a as a function of the normalized distance, $z/d = Z/L$, for $d = 68$, 125, and 260 μm and for 10 μm s^{-1} < v_0 < 100 μm s^{-1}. The measurements for $d = 17$ μm could not be performed because of the lack of contrast at such a small distance. For higher d, the measurements were easier and more accurate. Some measurements at low translation speeds could also not be considered because of the importance of natural convection. All profiles deviate from linearity. The results can be surrounded by two power laws $v/v_0 = (z/d)^B$ with $1.1 < B < 1.8$.

Panels b and c or Figure 6 show respectively the simulated curves and the experimental points for $d = 68$ and 260 μm. Each
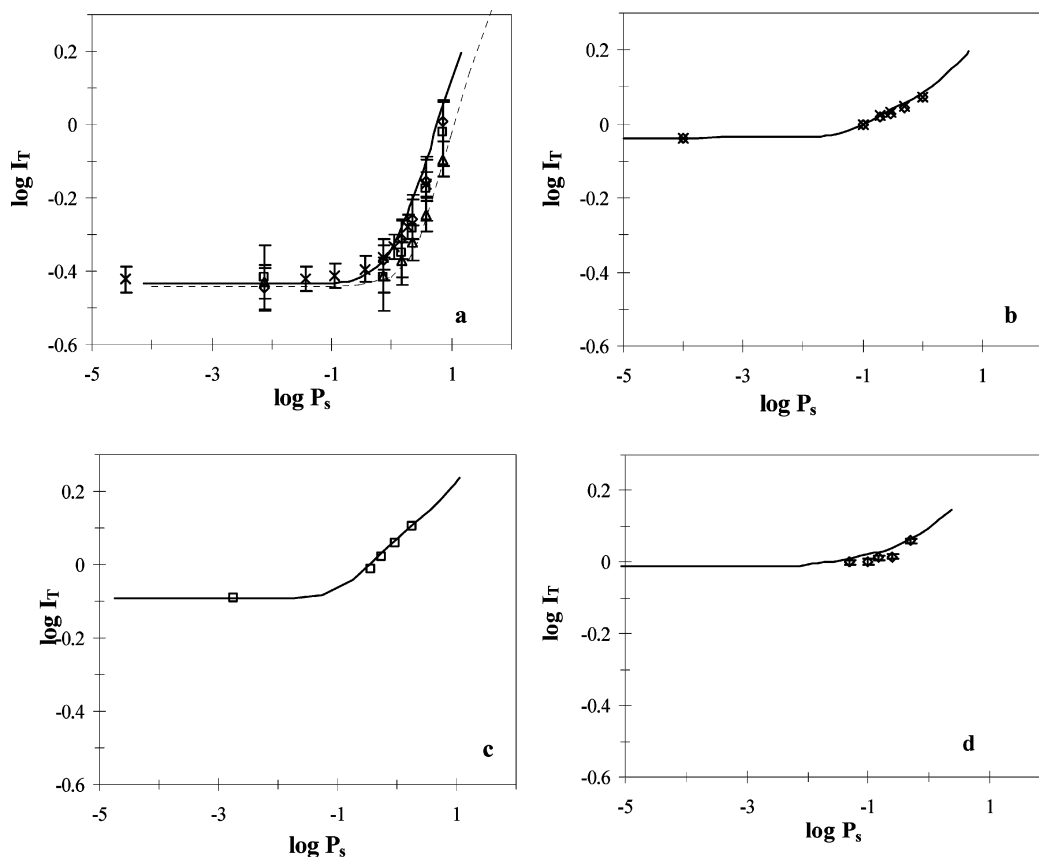
Figure 7. Comparison of experimental and simulated current profiles. Substrates: quartz (a−c); Petri (d). $d = 17$ (a), 68 (b), 125 (c), and 260 μm (d). —, simulated profiles for $RG = 10$. (a) - - - , simulated profile for $RG = 5$ and $d = 13$ μm; ×, experimental results interpreted with $D = 10^{-5}$ cm^2 s^{-1} instead of $D = 5 \times 10^{-6}$ cm^2 s^{-1}; $RG = 7.6$ (△) and 8.9 (□, ◇); for each curve, each symbol corresponds to the same series of measurements.

experimental point in Figure 6b,c corresponds to an average velocity for particles that are located between the tip and the bottom of the cell at the given altitude z. Indeed, the numerical calculation show, Figure 3, that the velocity is almost constant as long as $-1.2RG < x < 1.2RG$. According to the number of particles in a given focal plane during the measurement time, we have performed between two and seven measurements for a given z/d. The uncertainty bars given in Figure 6b,c are the corresponding standard deviations.

The discrepancy between the experimental and calculated values confirms the importance of the experimental difficulties encountered, as reported in the latter paragraph. The experimental uncertainty is higher for $d = 68$ μm than for $d = 260$ μm. This is due to errors on the real location of the particle. Such effect is smaller for $d = 260$ μm since then, the contrast is higher. This lack of accuracy makes the analysis of the results difficult. It is even impossible to deduce a tendency concerning the influence of d. We can only confirm the nonlinearity for $d > 68$ μm. The agreement between the simulations and the experiments is better for $d = 260$ μm. For $d = 68$ μm, the experimental deviation from linearity is higher than the simulated one. The trends predicted by the simulations are respected and a fair to good agreement is observed with experiments.

Electrochemistry at a Moving Tip. Tip Current. The microelectrode was held at a distance d from the insulating bottom of a cell containing an electroactive species. The tip was poised at a potential allowing the electrochemical transformation of the electroactive species under mass-transfer control. The current flowing through the tip for this transformation was monitored as the tip was moved horizontally above the substrate surface. A short delay of tens of seconds, depending on d and v_0, was required for the full steady development of the flow. For a fluid of viscosity η and density ρ, the evolution of the fluid velocity profile with time under Couette motion between plates separated by d tends toward a stationary state after a characteristic time, t, such as $(4/d)(\eta t/\rho)^{1/2} > 3$.[40] The steady flow development should then be reached in water or DMF within a fraction of a second. Once the movement was stopped, the current returned to its initial value more slowly than it had increased when the movement had started. The steady current of the moving tip is clearly higher than that at an immobile tip and increases as the tip speed increases.

Figure 7 presents the logarithmic variations of the experimental I_T, as a function of the Peclet number, P_s, obtained for different values of v_0 ($v_0 = 0$ and 1 μm s^{-1} < v_0 < 100 μm s^{-1}) and d (17, 68, 125, and 260 μm) for insulating substrates. For $d = 17$ and 260 μm, errors bars are indicated. They are deduced from the difference between the experimental and analytical I_T. We have compared the results to the simulated curve obtained for $RG = 10$ and indicated by the solid line.

There are some discrepancies between the theoretical and experimental values of the normalized current at an immobile tip.

(39) Bard, A. J.; Fan, F.-R. F.; Mirkin, M. V. In *Electroanalytical Chemistry*; Bard, A. J., Ed.; Marcel Dekker: New York, 1994; Vol. 18, p 243.
(40) Gooch, K. A.; Fisher, A. C. *J. Phys. Chem. B* **2002**, *106*, 10668.

At small distances, the discrepancy comes from the error in the tip−substrate separation d (this error is optimized from run to run so that $\Delta I_{T,exp}/I_{T,exp} < 10\%$). At higher distance, when the error in d is negligible (<1%), the discrepancy comes from the worse agreement between the theoretical and experimental approach curves at $L > 2$ (however, $(I_{T,exp} - I_{T,th})/I_{T,th} < 10\%$). We have translated the simulated curves from the logarithm of the ratio of those values, so that there is good match between the theoretical and experimental tip currents at $v = 0$.

In all cases, the electrode translation results in an increase of the current, which is all the more important as the electrode translation speed is higher.

For $d = 17\ \mu$m (Figure 7a), we have also used electrodes with different RG ratios while the normalized current of the immobile tip was kept at the constant value $I_T = 0.4$ within less than 10%. The difference in RG values at constant I_T corresponds to differences in tip−substrate separations, d. From numerical calculations, we show that $I_T = 0.4$ for $RG = 5$, $d = 13\ \mu$m and for $RG = 10$, $d = 17\ \mu$m. The effects of RG are taken into account in Figure 7a, and the points are compared to the simulated curves for $RG = 5$, $d = 13\ \mu$m and for $RG = 10$, $d = 17\ \mu$m (dashed line).

Three series of experimental measurements are reported (Figure 7a). The uncertainty, which can be evaluated by the error bars, corresponds to the positioning inaccuracy, which is important at such distance. The experimental series symbolized by the triangles corresponds to a lower RG ($RG = 7.6$) than those symbolized by the squares and the rhombs ($RG = 8.9$), which explains the lower values observed. The experimental points represented by the crosses correspond to the treatment of the data with $D = 10^{-5}$ cm^2 s^{-1} (phthalonitrile in DMF) instead of $D = 5 \times 10^{-6}$ cm^2 s^{-1} (Fe(CN)$_6^{4-}$ in water). The results show that, for the same tip speed, the increase in the tip current is lower for the species of lower D. However, in its dimensionless form, the process is independent of the diffusion coefficient. We may notice that all experimental dots are situated between the two simulation curves, which is satisfactory when one takes into account the uncertainty due to the position, d, the value of RG, and the diffusion coefficient, D.

For $d = 68$ and $125\ \mu$m, the agreement between the experimental points and the simulated curves is quite good. For $d = 260\ \mu$m, the agreement is not so good because of the variations of the stationary current, which are important in the case of the curved and flexible surface of the Petri box used as the substrate.

CONCLUSIONS

In SECM experiments, a tip is scanned above a surface and the motion of the tip induces a movement of the surrounding fluid that might perturb the electrochemical response of the electrode. We have studied the effect of a tip motion parallel to the substrate surface on the tip response. First we have estimated from numerical calculations the fluid velocity profile resulting from the tip movement. For small tip−substrate separations, $d \leq 2.72$, the flow generated by the tip motion is a linear shear flow (Couette flow). For larger separations ($d \geq 5$), the velocity profile deviates from this linear law as edges of the insulating part of the electrode become important.

We have then estimated from finite element calculations the influence of the fluid movement onto the electrochemical response of the electrode. We have solved the problem in the case of an isolated electrode and extended the results described in the literature. The presence of a conductive or an insulating substrate in the vicinity of the electrode, as in SECM experiments, alters the electrode response. Different mass-transfer regimes can be observed depending on the tip speed and the nature of the substrate. We have described those regimes and shown that when the tip moves faster than 10 μm s^{-1}, or in dimensionless form when $v_0 a/D \geq 0.06$, above an insulating substrate, the current response is perturbed by the motion. At large scan rates, the tip current loses its ability to discriminate between differences in substrate reactivity (insulating versus conducting).

These results show that particular attention should be taken when obtaining information from SECM imaging or when using SECM as a lithographic tool.

The theoretical results are confronted with experiments. The deviation from Couette flow is confirmed. The tip current increase due to the tip motion is clearly observed and quantified, and a good correlation with the numerical analysis is observed.

This work allows a better understanding and, if desired, a deeper analysis of both electrochemical reactivities and topographical images obtained by SECM.